Mathematical modelling of water and solute movement in ridged *versus* flat planting systems

S. J. DUNCAN[a], K. R. DALY[a], P. SWEENEY[b] & T. ROOSE[a]

[a]*Bioengineering Department, Faculty of Engineering & the Environment, University of Southampton, UK, SO17 1BJ, and* [b]*Syngenta, Jealott's Hill, Bracknell, UK, RG42 6EY.*

Correspondence: T. Roose. E-mail: T.Roose@soton.ac.uk

Running Title: Solute movement in ridge versus flat planting systems

Summary

We compared water and solute movement between a ridge and furrow geometry and that of flat soil with a mathematical model. We focused on the effects of two physical processes: root water uptake and pond formation on the soil surface. The mathematical model describes the interaction between solute transport, water movement and surface pond depth. Numerical simulations were used to determine how solutes of varying mobility and rates of degradation penetrated into the two soil geometries over a growing season. Both the ridge and furrow or flat soil geometries could reduce solute leaching, but this depended on several factors. Rain immediately after a solute application was a key factor in determining solute penetration into soil. In cases with delayed rain after a solute application, solutes in ridge and furrow geometries collected adjacent to the root system, resulting in reduced solute penetration compared to the flat soil geometry. In contrast, substantial rain immediately after a solute application resulted in ponding where water infiltration acted as the dominant transport mechanism. This resulted in increased solute penetration in the ridge and furrow geometry compared to the flat soil geometry.

Keywords: *Water movement, solute transport, ridge and furrow, flat field.*

Highlights

- We studied solute movement controlled by ponding in ridge and furrow and flat fields.
- We found the ridged soil could impede or increase leaching compared to the flat soil.
- Solute hot-spots formed in ridge and furrow soil because of root water uptake.

- Time between solute application and rainfall is a key factor for solute penetration.

Introduction

In arable farming several planting methods are used to cultivate crops (Fahong *et al.*, 2004). Two planting methods are addressed in this paper: ridge and furrow planting (Robinson, 1999) and flat planting (Lewis & Rowberry, 1973). A ridge and furrow geometry is formed when the soil surface is modified to form a periodic series of peaks (ridges) and troughs (furrows). This allows water to flow across the field providing water to the plants whilst preventing waterlogging of the roots (Tisdall & Hodgson, 1990). One crop that is traditionally grown in ridge and furrow geometries is the potato (*Solanum tuberosum*, L.) (Wayman, 1969), which is an essential crop in temperate European environments (Huaccho & Hijmans, 1999).

There have been several experimental efforts to determine the difference in potato growth and production between ridge and furrow planting and other tillage methods. Such methods include wide beds (Mundy *et al.*, 1999), flat planting (Lewis & Rowberry, 1973) and furrow only planting (Steele *et al.*, 2006). Both ridge and furrow and flat planting result in similar yields and tuber size (Lewis & Rowberry, 1973; Alva *et al.*, 2002), but ridge and furrow planting has been found to be the preferred method of tillage (Jordan *et al.*, 2013) because of ease of harvesting (Leistra & Boesten, 2010b), slow seed germination (Benjamin *et al.*, 1990) and nutrient replenishment in the soil (Feddes *et al.*, 1976).

Growing evidence suggests that ridge and furrow systems might be vulnerable to solute leaching (Lehrsch *et al.*, 2000; Alletto *et al.*, 2010; Kettering *et al.*, 2013). Experimentally, solutes have been applied to ridges and furrows of potato fields to determine the depth of solute penetration in different areas of the soil (Smelt *et al.*, 1981; Kung, 1988; Leistra & Boesten, 2010a). In these cases, the solute in the furrows moved to a greater absolute depth in soil, supporting the suggested vulnerability of the ridge and furrow geometry to solute leaching. Furthermore, a recent European Food Safety Authority report indicated that ridge and furrow soil surfaces can increase leaching six-fold compared to flat surfaces (EFSA, 2013). However, there is also evidence that ridge and furrow planting can reduce leaching if solute management techniques are used (Jaynes & Swan, 1999). These techniques can reduce the negative environmental effect (Hatfield *et al.*, 1998), even compared to flat planting (Ressler *et al.*, 1997).

In this study, we determine the water and solute movement mechanisms and key environmental factors that affect leaching in ridge and furrow, and flat planting systems. This will enable us to understand how the soil geometry affects transport within the soil. Understanding the key factors that affect solute leaching will allow us to determine qualitatively the increased risk to solute leaching between the two planting methods. This knowledge will assist us in developing solute application protocols unique to each planting method to reduce solute leaching and maintain greater nutrient availability to the crops.

Specifically, we modelled the transport of solutes with varying mobility and degradation in both soil geometries over 24-week periods. During this time, vegetation was present in soil for the first 16 weeks, i.e. a full growing season. Special attention was paid to ponding on the soil surface because we considered a temperate environment in the United Kingdom where there are often large amounts of rain. It should be noted that we assume that there is no solute uptake by plant roots. In this paper we are only concerned with the solute transport problem, i.e. modelling the ‘worst case scenario’, which applies directly to passive solutes.

Mathematical model

We used the water–solute–pond model developed in Duncan *et al*. (2018) to study water and solute movement in a cross section of a ridge and furrow (or flat) geometry. Here we state the equations and parameters used in the model, for a full derivation see Duncan *et al*. (2018). The governing equations are,

$$\phi\frac{\partial S(p)}{\partial t}+\boldsymbol{\nabla}\cdot\left\{-\frac{\kappa_{\mathrm{s}}}{\mu}S(p)^{\frac{1}{2}}\left[1-\left(1-S(p)^{\frac{1}{m}}\right)^{m}\right]^{2}\left(\boldsymbol{\nabla}p+\rho g\hat{\mathbf{k}}\right)\right\}=\begin{cases}-\lambda_{\mathrm{c}}(p-p_{\mathrm{r}}), & \mathbf{x}\in\Lambda_{\mathrm{U}}\\ 0, & \mathbf{x}\in\Lambda_{\mathrm{A}}\end{cases}, \tag{1}$$

$$\frac{\partial c}{\partial t}[b+S(p)\phi]+\frac{\partial p}{\partial t}\left\{\frac{\partial S(p)}{\partial p}\phi c\right\}+\boldsymbol{\nabla}\cdot[-D_{\mathrm{f}}\phi^{d+1}S(p)^{d+1}\boldsymbol{\nabla}c]+$$
$$\boldsymbol{\nabla}\cdot\left\{-\frac{c\kappa_{\mathrm{s}}}{\mu}S(p)^{\frac{1}{2}}\left[1-\left(1-S(p)^{\frac{1}{m}}\right)^{m}\right]^{2}\left(\boldsymbol{\nabla}p+\rho g\hat{\mathbf{k}}\right)\right\}=-\xi c,\quad \mathbf{x}\in\Lambda, \tag{2}$$

where ϕ is the soil porosity, $S(p)$ is the relative saturation, μ is the viscosity of water, p is the soil water pore pressure, ρ is the density of water, g is the acceleration due to gravity, $\hat{\mathbf{k}}$ is a unit vector in the upwards direction, κ_{s} is the saturated hydraulic permeability, m is a van Genuchten parameter, λ_c is the product of the root surface area density and water conductivity of the plant root cortex, p_{r} is the pressure in the root xylem, D_{f} is the diffusion coefficient in free liquid, d is the impedance factor of the solute that accounts for the tortuosity of the solute moving through the pore space, c is the solute concentration in the pore water, ξ is the solute decay rate constant related to bacterial and other degradation processes, b is the buffer power, Λ is a generalized ridge and furrow geometry (see Figure 1 in Duncan *et al*. (2018)) with subdomains Λ_{U} and Λ_{A} for regions where roots are present and absent respectively.

The boundary and initial conditions imposed on Λ are,

$$p = \rho g h(x,t), \quad \mathbf{x} \in \partial\Lambda_{\mathrm{P}}, \tag{3}$$

$$\mathbf{n} \cdot \left\{ \frac{\kappa_{\mathrm{s}}}{\mu} S(p)^{\frac{1}{2}} \left[1 - \left(1 - S(p)^{\frac{1}{m}} \right)^{m} \right]^{2} (\nabla p + \rho g \hat{\mathbf{k}}) \right\} = \min\{\Gamma(t), I_{\mathrm{c}}\}, \quad \mathbf{x} \in \partial\Lambda_{\mathrm{R}}, \tag{4}$$

$$\frac{dx_{\mathrm{o}}(t)}{dt} = f\left(R_{\mathrm{F}}(t), I_{\mathrm{f}}(t), R_{\mathrm{o}}(t)\right), \tag{5}$$

$$\mathbf{n} \cdot \left(\left[\mathrm{D_f} \phi^{d+1} S(p)^{d+1} \nabla c \right] + \left\{ \frac{c\kappa_{\mathrm{s}}}{\mu} S(p)^{\frac{1}{2}} \left[1 - \left(1 - S(p)^{\frac{1}{m}} \right)^{m} \right]^{2} (\nabla p + \rho g \hat{\mathbf{k}}) \right\} \right) = c_{\mathrm{m}}(t), \quad \mathbf{x} \in \partial\Lambda_{\mathrm{S}}, \tag{6}$$

$$\mathbf{n} \cdot \left\{ \frac{\kappa_{\mathrm{s}}}{\mu} S(p)^{\frac{1}{2}} \left[1 - \left(1 - S(p)^{\frac{1}{m}} \right)^{m} \right]^{2} (\nabla p + \rho g \hat{\mathbf{k}}) \right\} = 0, \quad \mathbf{x} \in \partial\Lambda_{\mathrm{E}} \cup \partial\Lambda_{\mathrm{W}}, \tag{7}$$

$$\mathbf{n}\cdot\left(\left[D_{\mathrm{f}}\phi^{d+1}S(p)^{d+1}\boldsymbol{\nabla}c\right]+\left\{\frac{c\kappa_{\mathrm{s}}}{\mu}S(p)^{\frac{1}{2}}\left[1-\left(1-S(p)^{\frac{1}{m}}\right)^{m}\right]^{2}\left(\boldsymbol{\nabla}p+\rho g\hat{\mathbf{k}}\right)\right\}\right)= 0,\quad \mathbf{x}\in\partial\Lambda_{\mathrm{E}}\cup\partial\Lambda_{\mathrm{W}}, \tag{2}$$

$$p=p_0,\quad \mathbf{x}\in\partial\Lambda_{\mathrm{B}}, \tag{9}$$

$$c=c|_{t=0},\quad \mathbf{x}\in\partial\Lambda_{\mathrm{B}}, \tag{30}$$

$$p|_{t=0}=p_{\infty}(\mathbf{x}),\quad \mathbf{x}\in\Lambda, \tag{4}$$

$$x_0(t)|_{t=0}=\eta, \tag{5}$$

$$c|_{t=0}=0,\quad \boldsymbol{x}\in\Lambda, \tag{13}$$

where $\partial\Lambda_{\mathrm{S}}$ is the soil surface boundary defined by the curve,

$$\chi(x)=A\cos(Bx)+C, \tag{14}$$

where A is the variation in soil depth, B is the ridge wave number and C is the average soil depth, $\partial\Lambda_{\mathrm{P}}$ is the region of $\partial\Lambda_{\mathrm{S}}$ where ponding occurs (see Figure 2 in Duncan *et al*. (2018)), $\partial\Lambda_{\mathrm{R}}$ is the region of $\partial\Lambda_{\mathrm{S}}$ that is not ponded, i.e. where rainfall penetrates the soil directly, and the interface between the two regions ($\partial\Lambda_{\mathrm{R}}$ and $\partial\Lambda_{\mathrm{P}}$) is defined by the moving boundary point $x_0(t)$ (see Figure 2 in Duncan *et al*. (2018)), $\partial\Lambda_{\mathrm{E}}$ and $\partial\Lambda_{\mathrm{W}}$ are the lateral boundaries of Λ, $\partial\Lambda_{\mathrm{B}}$ is the boundary at the base of Λ, $h(x,t)$ is the depth of the pond, $c_{\mathrm{m}}(t)$ is the volume flux of solute per unit soil surface area per unit time entering the soil domain, $\mathbf{n}$ is the unit normal vector pointing outwards of Λ, $\Gamma(t)$ is the volume flux of water per unit soil surface area, i.e. rainfall, I_{c} is the infiltration capacity of the soil, p_0 is the prescribed pressure at the base of the domain, η is the width of Λ, $R_{\mathrm{F}}(t)$ is rainfall landing directly into the pond, $I_{\mathrm{f}}(t)$ is the infiltration of water from the pond into the soil, $R_{\mathrm{o}}(t)$ is surface runoff, $c|_{t=0}$ is the initial solute concentration and $p_\infty(\mathbf{x})$ is the initial pressure profile.

Parameter values

There are 22 parameters in the model used in this study. These parameters are; $\phi, m, k_{\mathrm{s}}, \mu, g, \rho, p_{\mathrm{c}}, D_{\mathrm{f}}, d, b, \Gamma(t), c_{\mathrm{m}}(t), p_0, p_\infty(\mathbf{x}), \lambda_{\mathrm{c}}, \xi, p_{\mathrm{r}}$ and I_{c} for the coupled model, and the four parameters $A, B,$ C and η for the construction of Λ. These parameters are summarized in Tables 1 and 2.

Geometric, soil, environmental, plant and solute parameter values

To model the differences in solute and water movement between ridge and furrow and flat geometries, we construct two domains. These domains are shown in Figure 1, where Ω is the ridge and furrow geometry and Φ is the flat geometry. The flat geometry Φ can be reduced to a 1-D problem, however, for ease of comparison we present it as a 2-D geometry.

To replicate the dimensions of ridge and furrow geometries, we use the values $\eta = 0.5$ m, $A = C = \frac{1}{6}$ m and $B = 2\pi$ m^{-1} for the geometry Ω (Steele *et al.*, 2006; Li *et al.*, 2007). Furthermore, for the flat geometry we set $A = B = 0, C = \frac{1}{6}$ m and $\eta = 0.5$ m. To compare 'like for like' scenarios, we ensure that the ridge and furrow and flat geometries have the same total volume of soil.

Potatoes are a shallow-rooted crop in which the majority of roots are within the plough layer, i.e. the top 30 cm of soil (Lesczynski & Tanner, 1976). Therefore, in the ridge and furrow geometry we chose the size of the soil root region Ω_{U} to be the top 30 cm of soil extending radially from the top of the ridge. Similarly, for the flat soil geometry we chose the soil root region Φ_{U} to be the top 30 cm of soil (see Figure 1). There is a difference in the total root active soil between Ω_{U} and Φ_{U}, but this is taken into account when establishing the parameter for root length density (see below).

Several of the parameters in the model are dependent on the soil, including ϕ, m, k_s and p_c. Potatoes are a frequently grown in silt loam soil (Shock *et al.*, 1998). Therefore, we chose to use the parameter values for the 'Silt Loam G.E.3' soil from van Genuchten (1980), i.e. $\phi = 0.396$, $m = 0.51$, $k_\mathrm{s} = 5.2 \times 10^{-14}\ \mathrm{m}^2$ and $p_c = 23\,200$ Pa. Note that in some cases different tillage methods applied to soil can alter the porosity of the system. However, to ensure a 'like for like' comparison, we kept the porosity the same in both soil domains to ensure that any differences we observed were an effect of the soil geometry and not dependent on small variations in local porosity within the soil.

We took values from the literature for the environmental and fluid parameters. For the viscosity of water we used $\mu = 1 \times 10^{-3}\ \mathrm{kg\ m^{-1}\ s^{-1}}$, for acceleration due to gravity $g = 9.81\ \mathrm{m\ s^{-2}}$ and for the density of water $\rho = 1000\ \mathrm{kg\ m^{-3}}$.

The typical range of the impedance coefficient d is between 0.5 and 2 (Nye & Tinker, 1977). Furthermore, increased volumetric moisture content leads to an increase in the impedance factor for a solute (Rowell *et al.*, 1967). Given that we are modelling a temperate UK climate with frequent heavy rain events, we took d to be at the upper bound of this range, i.e. $d = 2$.

Values of the diffusion coefficient D_f in a solution of free liquid for simple electrolytes range from $1 \times 10^{-9} - 3 \times 10^{-9}\ \mathrm{m^2\ s^{-1}}$ (Shackelford & Daniel, 1991). Therefore, we chose the value to be in the middle of this range, i.e. $D_\mathrm{f} = 2 \times 10^{-9}\ \mathrm{m^2\ s^{-1}}$.

The parameter λ_c is the product of the root surface area density and the water conductivity of the root cortex, this can be expressed as

$$\lambda_c = k_{\mathrm{r}} l_{\mathrm{d}}(t), \tag{15}$$

where $l_{\mathrm{d}}(t)$ is the root length density and k_{r} is the radial conductivity of the root cortex per unit root length.

We simulated 24 weeks of solute and water movement in soil, in which vegetation was present for the first 16 weeks, which is typical for a potato crop (Noda *et al.*, 1997). For potato plants the root length density changes significantly over a 16-week growing period (Lesczynski & Tanner, 1976). Lesczynski & Tanner (1976) found that over the first 30 days the root length density develops to approximately $l_{\mathrm{d}} = 3 \times 10^4\ \mathrm{m\ m^{-3}}$ in the plough layer of soil. This then remains fairly constant until approximately 90 days, in which the root length density declines. To represent this growth and development, we assigned $l_{\mathrm{d}}(t)$ the piecewise function (in $\mathrm{m\ m^{-3}}$) as follows:

$$l_{\mathrm{d}}(t) = \begin{cases} 1 \times 10^3\, t & 0 \le t < 30 \text{ days} \\ 3 \times 10^4 & 30 \le t < 90 \text{ days} \\ 3 \times 10^4 - (1 \times 10^3) \times (t - 90) & 90 \le t < 120 \text{ days} \\ 0 & 120 < t \text{ days} \end{cases}. \quad (16)$$

These results were obtained with ridge and furrow planting, therefore we must account for this when determining a root length density function for the flat soil geometry. To have the same total root length in Ω and Φ, we scale $l_{\mathrm{d}}(t)$ in the flat geometry by the ratio of the two root active areas Ω_{U} and Φ_{U}. This ensures a ‘like for like’ comparison between the two geometries.

For maize (*Zea mays,* L.) roots, the parameter k_{r} is given the value $7.85 \times 10^{-10}\ \mathrm{m^2 s^{-1} MPa^{-1}}$ (Roose & Fowler, 2004a). Maize and potato roots have similar root radii and structure (Rawsthorne & Brodie, 1986; Steudle *et al.*, 1987), therefore we assumed that this value of k_{r} is also representative of potato roots in soil.

To describe root pressure p_{r}, there are models for root pressure distribution within a single root (Roose & Fowler, 2004a). However, to simulate large areas of soil consisting of many roots, we used an average root pressure to describe the plant root system. The root pressure p_{r} can vary considerably in potatoes depending on several factors including soil saturation and atmospheric conditions (Gandar & Tanner, 1976). Liu *et al.* (2006) found that the root water potential changed considerably based on the method of irrigation applied to the crop. They found that p_{r} was ≈ -0.01 MPa in the roots of a fully irrigated system and $\approx (-0.02, -0.2)$ MPa for areas of soil with partial root drying. Given that we model frequent rain events that promote ponding, we chose the value $p_{\mathrm{r}} = -0.05$ MPa.

The infiltration capacity I_{c} of soil depends on several factors, including volumetric water content, soil type and tillage methods (Azooz & Arshad, 1996). Therefore, it is difficult to assign a single value to the infiltration capacity of a soil. Morin & Benyamini (1977) found that steady state infiltration of bare loam soil was reached after approximately 20 minutes into a rain event. However, the rain data we used (see *Rainfall and solute application parameter values*) has a time resolution of 1 hour, which is considerably larger than the time required to reach steady state infiltration. Therefore, we averaged the infiltration capacity over each rain event. Morin & Benyamini (1977) found that the steady state rate of infiltration of bare loam soil is between $1.3 - 2.2 \times 10^{-6}$ m s^{-1}. Given this, we chose to assign the value $I_{\mathrm{c}} = 1.3 \times 10^{-6}$ m s^{-1}.

We show results of numerical simulations for multiple hypothetical solutes with varying rates of degradation and buffering capacity to determine the differences in solute movement between the ridge and furrow and flat soil geometries. In Table 2 we give a matrix of the solute parameters that are used in the simulations.

We chose to model extremely mobile solutes $(\alpha_1, \alpha_2, \alpha_3)$ with a buffer power of $b = 0.1$, highly mobile solutes $(\beta_1, \beta_2, \beta_3)$ with a buffer power of $b = 1$ and moderately mobile solutes $(\gamma_1, \gamma_2, \gamma_3)$ with a buffer power of $b = 10$.

It is generally accepted that rates of degradation of pesticide-like solutes in soil decrease with depth (Fomsgaard, 1995). Therefore, one value for the decay constant is not valid for the entirety of the soil domains in Figure 1. For the pesticides Isoproturon and Metolachlor, the half-life is approximately doubled between the initial 0–30cm of soil and 1m below the soil surface (Rice *et al.*, 2002; Bending & Rodriguez-Cruz, 2007). Hence, for spatially varying degradation, we impose the function,

$$t_\lambda(\mathbf{x}) = t_\lambda^* + |z_{\mathrm{A}}| t_\lambda^*, \qquad (17)$$

where, t_λ^* is the half-life of the solute in the plough layer and $|z_A|$ is the absolute depth below soil surface.

For the rapidly degrading solutes $(\alpha_1, \beta_1, \gamma_1)$ we chose the value for the half life $t_\lambda^* = 10$ days, for a moderately fast degrading solute $(\alpha_2, \beta_2, \gamma_2)$ we selected the value $t_\lambda^* = 50$ days and for slowly degrading solutes $(\alpha_3, \beta_3, \gamma_3)$ we selected the value $t_\lambda^* = 500$ days. It follows that the half-life t_λ^* relates to the solute decay constant ξ by

$$\xi = \frac{\ln(2)}{t_\lambda(\mathbf{x})}. \qquad (18)$$

Boundary and initial condition parameters values

For the parameter p_0 that describes a constant saturation at the base of the geometry, we assigned the pressure value $p_0 = -10$ kPa. This equates to a saturation level of approximately $S \approx 0.9$ for a silt loam soil, thereby replicating a shallow water table. For the soil water pore pressure initial condition $p_\infty(\mathbf{x})$, we chose to impose the steady state profile that forms when the domain has no plant roots. As a result of capillary forces and gravity, this leads to a constant pressure gradient from the base to the top of the geometry, such that

$$p_\infty(\mathbf{x}) = -p_\infty^{\mathrm{m}} z - p_\infty^{\mathrm{c}}, \quad \mathbf{x} \in \Omega \cup \Phi, \qquad (19)$$

where $p_\infty^{\mathrm{m}} = 9825$ Pa and $p_\infty^{\mathrm{c}} = 19{,}825$ Pa.

Rainfall and solute application parameter values

We simulated solute and water movement over a 24-week period, in which vegetation was present for the first 16 weeks. Potatoes are typically planted from April to June and are harvested in September to November (Noda *et al.*, 1997). Therefore, we simulated this ‘growth and harvesting' timeframe with an additional 8 weeks to determine how solutes move once the crops are harvested.

For the volume flux of water per unit soil surface area $\Gamma(t)$, i.e. rainfall, we used 6 months of rain field data from a site in Newbury, UK between 1 June 2006 and 31 December 2006. These data are shown in Figure 2. The data were recorded from instruments that were installed on a slope next to the A34 Newbury bypass (Ordnance Survey grid reference SU455652). Acquisition of the data is described in (Smethurst *et al.*, 2006).

We applied the solutes at one of two times during the numerical simulations, these are denoted as the early and late applications. For the early application, solute was applied to the soil surface at the start of the simulation over the initial 24 hours, with a total application of 1 $\mathrm{kg\ ha^{-1}}$, i.e. an application rate of $c_m(t) = 1.157 \times 10^{-9}\ \mathrm{kg\ m^{-2}\ s^{-1}}$. Similarly, for the late application a solute was applied for 24 hours with the same rate of application at the beginning of the 15th week. These can be seen in Figure 2. The early and late application times where chosen to determine how solute movement is affected during a growing and degrading root system, respectively. For the early application, the solute was applied as soon as the root system began to grow and the late application was applied shortly after the root length density began to decrease.

Results

We did a total of 36 simulations; nine simulations for the ridged geometry with an early application (for all nine hypothetical solutes in Table 2), nine for the ridged geometry with a late application, nine for the flat geometry with an early application and nine simulations for the flat geometry with a late application.

Early application results

Figure 3 shows the results for the early application of solutes for both the ridged and flat planting systems for the moderately mobile solutes, i.e. solutes γ_1, γ_2 and γ_3 (see Table 2). The results in Figure 3 show the solute profiles in the two soil geometries at 16 and 24 weeks after the solute application. At 16 weeks after the solute application, water uptake from vegetation stops because this simulates harvesting and the removal of crops, and 24 weeks after solute application is the end of the simulation timeframe. Furthermore, an additional contour plot of concentration $10\ \mu\text{g l}^{-1}$ (shown in white) was added to each profile; because this concentration is frequently used as a pesticide safety threshold for root and tuber vegetables (EU, 2018). In Figures 4 and 5 we show the results for the highly mobile ($\beta_1, \beta_2, \beta_3$) and extremely mobile ($\alpha_1, \alpha_2, \alpha_3$) solutes, respectively.

For the moderately mobile solutes ($\gamma_1, \gamma_2, \gamma_3$), there was no significant penetration of the solutes into either of the soil geometries because of the buffer power of the solutes (see Figure

3). However, several features of the solute movement can be identified. First, the solute adjacent to the furrow has penetrated deeper into the soil than that contained in the ridge. Experimentally, deep furrow penetration has been attributed to the effects of ponding in the furrow of the geometry from soil surface runoff (Leistra & Boesten, 2010a), which is evident in the simulation results.

Furthermore, we note that because roots take up water, solute is drawn up towards the ridges through the difference between the soil water pore pressure and pressure in the root system. Chen *et al*. (2011) found that in ridge and furrow structures, water that infiltrated into the furrows of the system was transported to the ridges, which in turn reduced water movement directly below the ridge. In the simulations, this resulted in greater concentrations of solute in the ridges of the system from water transporting the solute. This coincides with the results of Smelt *et al.* (1981), who found that most solute residues were in the ridges of the ridge and furrow structures at the end of the growing season. Similarly, Jaynes & Swan (1999) found substantially larger concentrations in the ridges of the structure than the furrows.

In the flat soil geometry, the solute moved down uniformly and was temporarily impeded by the roots in the plough layer. When we compared the solute penetration between the flat and ridged soils, we found that the solute in the flat geometry moved to a greater absolute depth below the soil surface than that in the ridges. This result concurs with that of Hamlett *et al*. (1990), who identified that placing solutes on the ridges of the structure substantially reduced the amount leached compared to the flat field application. Jaynes & Swan (1999) supported this hypothesis, and in addition found that applications to the ridges could provide increased quantities of solute to the plant, i.e. nutrients and fertilizers.

We observed, however, that the solute in the flat soil penetrated less than that in the furrows of the ridged soil. This can be explained by the distribution of ponding on the two soil geometries. When ponding occurred on the flat soil, the ponding depth was considerably shallower than on the ridged soil because the pond was uniformly spread over the entire soil surface, whereas, for the ridged soil the pond was only in the furrow. This in turn, causes a greater body of water to infiltrate into the furrow, causing deep solute penetration in this region of the geometry, but reducing the penetration of solutes in the ridges of the geometry.

Similar properties are evident in Figure 4 (for the solutes $\beta_1, \beta_2, \beta_3$) and Figure 5 (for the solutes $\alpha_1, \alpha_2, \alpha_3$) for the simulations containing highly and extremely mobile solutes. For the highly mobile solutes β_1, β_2 and β_3 in the ridged system (Figure 4), the effect of solute accumulation in the ridges is more pronounced. In the ridge simulation containing solute β_3 at 16 weeks post solute application, there is a large quantity of solute in the region of soil adjacent to the plant roots because of water transport to the ridges created by the ridge and furrow geometry (Bargar *et al.*, 1999; Chen *et al.*, 2011).

At 24 weeks (the end of the simulation), the solute has penetrated into the soil as a concentrated spot that diffuses out slowly. We know that solute movement was reduced there when there was root uptake in soil (Benjamin *et al.*, 1996). Roots are only present for the first 16 weeks, therefore, for the remaining 8 weeks the solute is affected more by rainfall into the ridges. Hence, we observed deeper solute penetration in the later portion of the simulation. Furthermore, we note that for the highly degrading solute β_1, the concentration decreased below the $10\ \mu g\ l^{-1}$ threshold for both soil geometries. This was due to the combination of fast dispersion and short half-life. In either geometry, it is the slowly degrading solutes $(\alpha_3, \beta_3, \gamma_3)$ that are of critical importance.

Figure 5 shows the results for the extremely mobile solutes α_1, α_2 and α_3. For the solute α_3, we found that a quantity of solute left the base of both soil geometries. In the ridge simulation, as an effect of the solute accumulating in the ridges, the solute moved down the soil profile as a highly concentrated spot. Given that the solute was drawn up into the ridges early in the simulation, the majority of the solute was not affected by later ponding in the furrows. Therefore, the solute moved down solely under the influence of the rain that entered the ridge of the soil, and takes longer to reach the base of the geometry. In the flat geometry, however, all of the solute was affected by ponding (albeit considerably less than in the furrow of the ridged soil). This led to large quantities of the solute reaching the base of the geometry. The total amount of solute that crossed the base of the geometry was 0.26 mg in the ridged system and 3.5 mg in the flat system. These findings support the results observed by Hamlett *et al*. (1990) and Jaynes & Swan (1999), who found that placing solutes on the ridges of the structure substantially reduced leaching compared to the flat field application. Applying solute solely to the ridges negated the effects of ponding, which reduced the penetration depth in the soil. Furthermore, root uptake reduced solute movement in the ridges (Benjamin *et al.*, 1996). This caused the solute to remain near the surface, allowing for easy solute extraction from the soil after harvesting.

In the ridge and furrow simulations, we observed that as an effect of water uptake from plant roots, movement of the solute from the furrow to the ridges protected the solute from deep penetration which would otherwise result from furrow ponding. Flat ground has a uniform surface that offered no protection, therefore all the solute was affected by ponding and rainfall. Therefore, the average depth of the solute was reduced in the ridged soil compared to the flat soil when this solute movement mechanism was present.

Late application results

Figure 6 shows the solute profiles for the early and late applications of the solutes α_3, β_3 and γ_3, i.e. those with slow degradation, in the two soil geometries at the end of the simulations. For simulations with the early application the solutes were in the soil for a full 24 weeks, and for the late application the solutes were in the soil for 9 weeks. We chose to show the results of the slowly degrading solutes only because they showed the most extreme behaviour and highlight the effects of surface ponding best. Nevertheless, the other solutes showed a similar qualitative behaviour.

From the results in Figure 6 we can highlight several key features. In the simulations with the late application of solutes α_3, β_3 and γ_3 in the ridge and furrow geometry, a substantial quantity of solute penetrates into the furrow. This is considerably different from the simulations of solute profile in the early application to the ridge and furrow, in which the solutes move towards the ridge and form a concentrated spot.

There appear to be three reasons for differences in the solute profiles between the early and late applications to the ridge and furrow soil. First, for the late application simulation, the time that the solute was in the soil was less than for the early application. Therefore, in simulations of the late application there was not as much time for the solute to be transported towards the ridge of the structure by water that infiltrated into the furrows and moved to the ridges (Bargar *et al.*, 1999; Chen *et al.*, 2011). Second, for the late application the root length density was beginning to decline such that the root uptake was not as strong as earlier in the simulated growing season (refer to Equation (16)). Consequently, the difference in the soil water pore pressure between the ridge and the furrow decreased, which resulted in less movement of water and solute towards the ridge and greater solute penetration (Benjamin *et al.*, 1996). The third reason for the reduction in spot formation was rain that occurred immediately after the late application. Figure 2 shows that there was an intense rain event shortly after the late application, which caused considerable ponding in the furrow of the soil. Given that the solute had been applied recently to the soil, there had not been sufficient time for it to collect in the ridges. Therefore, the solute contained in the region of soil adjacent to the furrow moved deep into the soil by water infiltration from the pond because surface runoff leading to pond infiltration acts as a key transport mechanism for the solute (Leistra & Boesten, 2010a).

From the rainfall data shown in Figure 2, we can see that during the second three-month period (representing the winter months) there are more frequent 'high-intensity' rain events than during the first three months. In simulations of the late application, this caused solute in the furrow of the ridged geometry to move deep into the soil and did not allow formation of a spot in the ridges. This made the solute in the furrow vulnerable to leaching because large amounts of water infiltration can generate substantial dispersion of solutes in ridged soil (Abbasi *et al.*, 2004). The effect of the 'time of ponding' is evident in the difference between the simulation results for early and late applications of the solute α_3 in the ridged soil. In the early application, the solute collected in the ridges of the system because of little ponding and a growing root system, and then proceeded to move down as a concentrated spot as the root length density decreased. For the late application with immediate surface ponding and a lack of roots, the solute moved down the profile with a wider distribution under the influence of infiltration of water from the pond.

For the simulations of the extremely mobile solute α_3, in several cases some solute left the system from the base of the geometry. Furthermore, the total quantity that crossed the base of the domain depended on the soil geometry and time of application. In simulations of the early application, 0.26 mg of solute leached in the ridge geometry, whereas it was 3.5 mg for the flat system. For the late application, however, the amount leached was 0.15 mg in ridge geometry and it was zero in the flat system.

The model results suggest that the optimal geometry to reduce solute leaching depends on two key aspects: the immediate rainfall regime after solute application, and the quantity of roots in the soil. In simulations of the early solute application, the amount of rain was not sufficient to generate substantial furrow ponding. This allowed the solute to move towards the ridges of the system under the influence of water movement, which is often observed in ridge and furrow soils (Bargar *et al.*, 1999; Chen *et al.*, 2011). This protects the solute from future furrow ponding because root uptake can reduce solute movement in the ridges (Benjamin *et al.*, 1996). In contrast, for simulations of the late application there was an immediate heavy rain event after solute application that caused substantial ponding. This generated more ponding in the ridged than the flat soil, which resulted in the solute in the furrow being transported deeper into the soil. This made the ridge and furrow system substantially more vulnerable to solute leaching than the flat soil. Therefore, substantial rain that causes ponding after a solute application may make the ridged system more susceptible to solute leaching.

Time of rain versus solute leaching

From the results above, we ran a series of simulations to test the hypothesis that the time between solute application and a heavy rain event influences the quantity of leaching in ridged soil. We set up five ridged and five flat soil simulations in which a solute (with the same properties as the solute α_3) was applied uniformly to each soil. One heavy rain event that would generate substantial ponding was then simulated at different times after the solute application in each simulation. The rain event was chosen to last for 4 hours and have a rainfall intensity of 12 mm hr^{-1}, and the times between solute application and the rain event were chosen to be 1, 2 and 4 days, 1 and 2 weeks. One day after the rain event, the total amount of solute that crossed the plough layer was then calculated. The plough layer was chosen to be the soil above the horizontal line of -0.15 m in both soil geometries shown in Figure 1.

Figure 7 shows the total amount of solute (as a percentage of solute applied) that crossed the horizontal line of -0.15 m in the soil geometries. For the simulations where the heavy rain event was 1 day after solute application, there were trace amounts of leaching in the flat geometry. However, in the ridged geometry 11% of solute applied leached past the plough layer.

In the simulations for longer periods of time between the solute application and the rain event, the relation between the amounts of solute that were leached in the two geometries changed. In the ridge and furrow simulations, as the time between solute application and rain event increased more of the solute moved towards the ridges of the soil by water transport from the furrows (Chen *et al.*, 2011). This caused less solute to be affected by the ponding and water infiltration from the heavy rain event, and less solute moved below the plough layer. For example, when the time period between solute application and rain was 14 days, approximately 1.5% of the solute applied was leached below the plough layer.

The flat geometry, however, showed the opposite behaviour. As the time between solute application and the rain event increased, more solute was leached past the plough layer. This resulted from solute diffusion in the system before the rain event. We simulated an extremely mobile solute, therefore the longer it was in the system the more it diffused. This meant that the rain and pond infiltration had a greater effect on transport of the solute. In the simulation with a 14-day period between solute application and the rain event, the total amount of solute leached was approximately 11%.

Figure 7 illustrates a crossover between the total quantities of solute leached in the plough layer for the two geometries after approximately 8 days. In the case study of an extremely mobile solute and a single heavy rain event in a silt loam soil, there was less than 8 days between solute application and the rain event and the flat geometry reduced leaching more. However, with more than 8 days between solute application and rain, the ridge and furrow geometry reduced leaching more than for the flat geometry because the solute moved towards the ridges and created a 'zone of protection' from ponding. This crossover period, however, can change considerably depending on the mobility of solute, rainfall regime and type of plant roots. For example, in scenarios where the applied solute is less mobile and root densities in the soil are less, the time for ridge accumulation will be longer, thereby delaying the crossover period. Nevertheless, these results suggested that specific situations determine whether the ridge and furrow or the flat soil are better at reducing leaching.

Discussion

In previous research, ridge and furrow planting has often been shown to lead to greater leaching of solutes than the flat system (Lehrsch *et al.*, 2000; Alletto *et al.*, 2010; Kettering *et al.*, 2013). However, certain application procedures might reduce leaching in ridged fields more than in flat fields (Ressler *et al.*, 1997; Hatfield *et al.*, 1998; Jaynes & Swan, 1999). This latter supports our findings; we observed that water movement from the furrows to the ridges (Bargar *et al.*, 1999) can transport solutes into the adjacent root zones of the structure and while held there by plant roots (Benjamin *et al.*, 1996) they reduced the effect from dominant surface runoff and subsequent infiltration (Leistra & Boesten, 2010a). Thereby, ridge and furrow systems can reduce solute leaching.

We made several key assumptions, however, to ensure that any differences observed depended on the geometry, i.e. by comparing the ridge and furrow and flat geometries directly. Therefore, it might be of interest to incorporate specific factors of ridge and furrow geometry to determine the magnitude and severity of the mechanisms that were observed.

One of the key factors to consider is the soil water content in each of the ridge and furrow and flat geometries. Water movement is the key transport mechanism for solutes in soil (Nye & Tinker, 1977), therefore it is vital to characterize the soil water profile accurately in both the ridge and furrow and flat soil geometries. In the mathematical model, we imposed a boundary condition at the base of the domains to replicate a shallow water table approximately 1 m below the soil surface. This allowed us to model solute movement within an idealized soil domain. However, with high spatial resolution field data to determine the soil water profile in the ridge and furrow and flat geometries we could indicate how different water profiles might affect the solute dynamics and mechanisms that we observed, i.e. solute penetration from furrow ponding and transport to the ridges from the furrow.

Understanding the water profile in soil would aid accurate determination of the infiltration mechanics of rain into the soil. We used rainfall data with a resolution of one hour for a 6-month period, which limits the accuracy of identifying any change in infiltration capacity. This could play a key role in determining the severity of ponding and therefore the movement of solutes from the furrow to the ridges. Thus, understanding the infiltration capacity and soil water content with higher temporal and spatial resolution might aid our understanding of the magnitude of the effects observed.

Coupling knowledge of the water profile with the antecedent moisture conditions of the soil domains would enable us to model the movement of solutes applied to the soil more accurately. We modelled the initial water profile to be that formed under steady state conditions in the absence of roots, which is unlikely to resolve true field conditions accurately. Knowledge of past conditions would enable us to determine accurate initial conditions for the soil at the beginning of the simulations. This information could have a marked effect on several factors such as the infiltration capacity, water table height and initial solute movement.

To understand further observed solute accumulation and hot spot formation mechanisms, knowledge of the root architecture would play a key role. This would enable us to understand the distribution of root pressures in the root zones, i.e. the ridges of the system, and to predict the spatial distribution of solutes that collect in the ridges of the soil geometry. This would provide a more quantitate analysis of specific case studies relating to different solutes and root systems.

Earlier, we stated that to obtain a 'like for like' comparison, we kept the porosity between the ridge and furrow and flat systems the same. However, we know that some tillage methods can affect the porosity of the soil. Therefore, it would be useful to determine how any effect from tillage would affect solute movement from the furrows to the ridges and also spot formation in the ridges. This could have a substantial effect on the time required for the solute in the furrows to move to the ridges of the system.

Conclusions

Our modelling results bridged the gap between two contrasting findings for ridge and furrow systems because previous literature suggested that these soil systems may be vulnerable to solute leaching, or can reduce solute leaching. We found the ridge and furrow structure could either impede or increase the penetration of solutes in soil depending on the rainfall activity immediately after solute application and the quantity of roots in the soil. In scenarios where there was considerable rain that generated substantial ponding immediately after solute application, we found that water infiltration from the surface acted as a strong transport mechanism for solutes in the furrow. This caused solutes in the furrow to move to a greater depth compared to the flat ground profile where the effect of ponding was less substantial.

We found, however, these trends were reversed when there was no ponding after solute application. Instead, roots in the ridges caused a dominant pressure gradient to form between the soil water pore pressure and pressure in the root xylem. This, caused the solute in the ridged system to move towards the soil with abundant roots, where the solute accumulated adjacent to the root zone in the ridges. This effect impeded the movement of the solute compared to the flat field because solute was in the ridge and therefore is not influenced by future ponding events in the furrow.

We determined that the vulnerability of the ridged system stemmed from immediate ponding on the soil surface after the application of a solute, and was not a function of the surface topology itself. Our results suggested that one of the important factors that should be considered when applying solutes to the soil surface is the immediate water treatment, i.e. rainfall or irrigation after the solute application as this can have a substantial influence on solute penetration and leaching in ridged fields.

Acknowledgements

SJD acknowledges a receipt of BBSRC Syngenta Case PhD studentship BB/L5502625/1,

TR and KRD are funded by ERC Consolidation grant 646809 DIMR.

Image data for the figures presented in this paper are available at the University of Southampton ePrints depository XXXXXX

Commented [DS1]: We will have a depository number from our library once the paper is formally accepted.

Conflict of Interest Statement:

Paul Sweeney is an employee of Syngenta Ltd and Simon Duncan is funded by BBSRC Syngenta Case PhD studentship.

References

Abbasi, F., Feyen, J. & van Genuchten, M.T. 2004. Two-dimensional simulation of water flow and solute transport below furrows: model calibration and validation. *Journal of Hydrology*, **290,** 63-79.

Alletto, L., Coquet, Y., Benoit, P., Heddadj, D. & Barriuso, E. 2010. Tillage management effects on pesticide fate in soils. A review. *Agronomy for sustainable development*, **30,** 367-400.

Alva, A.K., Hodges, T., Boydston, R.A. & Collins, H.P. 2002. Effects of irrigation and tillage practices on yield of potato under high production conditions in the Pacific Northwest. *Communications in Soil Science and Plant Analysis*, **33,** 1451-1460.

Bargar, B., Swan, J. & Jaynes, D. 1999. Soil water recharge under uncropped ridges and furrows. *Soil Science Society of America Journal*, **63,** 1290-1299.

Bending, G.D. & Rodriguez-Cruz, M.S. 2007. Microbial aspects of the interaction between soil depth and biodegradation of the herbicide isoproturon. *Chemosphere*, **66,** 664-671.

Benjamin, J., Ahuja, L. & Allmaras, R. 1996. Modelling corn rooting patterns and their effects on water uptake and nitrate leaching. *Plant and soil*, **179,** 223-232.

Benjamin, J., Blaylock, A., Brown, H. & Cruse, R. 1990. Ridge tillage effects on simulated water and heat transport. *Soil and Tillage Research*, **18,** 167-180.

Chen, X., Zhao, X., Wu, P., Wang, Z., Zhang, F. & Zhang, Y. 2011. Water and nitrogen distribution in uncropped ridgetilled soil under different ridge width. *African Journal of Biotechnology*, **10,** 11527-11536.

Duncan, S., Daly, K., Sweeney, P. & Roose, T. 2018. Mathematical modelling of water and solute movement in ridge plant systems with dynamic ponding. *European Journal of Soil Science*, **69,** 265-278.

EFSA. 2013. Scientific Opinion on the report of the FOCUS groundwater working group (FOCUS, 2009): assessment of lower tiers. *EFSA Journal*, **11,** 3114.

EU. 2018. Commision Regulation (EU) 2018/78 of 16 January 2018 amending Annexes II and III to Regulation (EC) No 396/2005 of the European Parliament and of the Council as regards maximum residue levels for 2-phenylphenol, bensulfuron-methyl, dimethachlor and lufenuron in or on certain products *Official Journal of the European Union***,** 6-30.

Fahong, W., Xuqing, W. & Sayre, K. 2004. Comparison of conventional, flood irrigated, flat planting with furrow irrigated, raised bed planting for winter wheat in China. *Field Crops Research*, **87,** 35-42.

Feddes, R.A., Kowalik, P., Kolinska-Malinka, K. & Zaradny, H. 1976. Simulation of field water uptake by plants using a soil water dependent root extraction function. *Journal of Hydrology*, **31,** 13-26.

Fomsgaard, I.S. 1995. Degradation of pesticides in subsurface soils, unsaturated zone—a review of methods and results. *International journal of environmental analytical chemistry*, **58,** 231-245.

Gandar, P. & Tanner, C. 1976. Potato leaf and tuber water potential measurements with a pressure chamber. *American Potato Journal*, **53,** 1-14.

Hamlett, J., Baker, J. & Horton, R. 1990. Water and anion movement under ridge tillage: a field study. *Transactions of the ASAE*, **33,** 1859-1866.

Hatfield, J.L., Allmaras, R.R., Rehm, G.W. & Lowery, B. 1998. Ridge tillage for corn and soybean production: environmental quality impacts. *Soil and Tillage Research*, **48,** 145-154.

Huaccho, L. & Hijmans, R.J. 1999. *A global geo-referenced database of potato distribution for 1995-1997 (GPOT97)*. International Potato Center (CIP).

Jaynes, D.B. & Swan, J. 1999. Solute movement in uncropped ridge-tilled soil under natural rainfall. *Soil Science Society of America Journal*, **63,** 264-269.

Jordan, M.O., Kelling, K.A., Lowery, B., Arriaga, F.J. & Speth, P.E. 2013. Hill Shape Influences on Potato Yield, Quality, and Nitrogen Use Efficiency. *American Journal of Potato Research*, **90,** 217-228.

Kettering, J., Ruidisch, M., Gaviria, C., Ok, Y.S. & Kuzyakov, Y. 2013. Fate of fertilizer 15N in intensive ridge cultivation with plastic mulching under a monsoon climate. *Nutrient cycling in agroecosystems*, **95,** 57-72.

Kung, K. 1988. Ground truth about water flow pattern in a sandy soil and its influences on solute sampling and transport modeling. In: *International conference and workshop on the validation of flow and transport models for the unsaturated zone* (eds. Wierenga, P. & Bachelet, D.), pp. 224-230. New Mexico State Univ., Las Cruces, NM.

Lehrsch, G.A., Sojka, R. & Westermann, D. 2000. Nitrogen placement, row spacing, and furrow irrigation water positioning effects on corn yield. *Agronomy Journal*, **92,** 1266-1275.

Leistra, M. & Boesten, J.J. 2010a. Measurement and computation of movement of bromide ions and carbofuran in ridged humic-sandy soil. *Archives of environmental contamination and toxicology*, **59,** 39-48.

Leistra, M. & Boesten, J.J. 2010b. Pesticide leaching from agricultural fields with ridges and furrows. *Water, Air, & Soil Pollution*, **213,** 341-352.

Lesczynski, D.B. & Tanner, C.B. 1976. Seasonal variation of root distribution of irrigated, field-grown Russet Burbank potato. *American Potato Journal*, **53,** 69-78.

Lewis, W.C. & Rowberry, R.G. 1973. Some effects of planting depth and time and height of hilling on Kennebec and Sebago potatoes. *American Potato Journal*, **50,** 301-310.

Li, X., Su, D. & Yuan, Q. 2007. Ridge-furrow planting of alfalfa (Medicago sativa L.) for improved rainwater harvest in rainfed semiarid areas in Northwest China. *Soil and Tillage Research*, **93,** 117-125.

Liu, F., Shahnazari, A., Andersen, M.N., Jacobsen, S.-E. & Jensen, C.R. 2006. Physiological responses of potato (Solanum tuberosum L.) to partial root-zone drying: ABA signalling, leaf gas exchange, and water use efficiency. *Journal of Experimental Botany*, **57,** 3727-3735.

Morin, J. & Benyamini, Y. 1977. Rainfall infiltration into bare soils. *Water Resources Research*, **13,** 813-817.

Mundy, C., Creamer, N., Crozier, C. & Wilson, L.G. 1999. Potato production on wide beds: Impact on yield and selected soil physical characteristics. *American Journal of Potato Research*, **76,** 323-330.

Noda, T., Takahata, Y., Sato, T., Ikoma, H. & Mochida, H. 1997. Combined effects of planting and harvesting dates on starch properties of sweet potato roots. *Carbohydrate Polymers*, **33,** 169-176.

Nye, P.H. & Tinker, P.B. 1977. *Solute movement in the soil-root system*. Univ of California Press, Berkeley and Los Angeles, California.

Rawsthorne, D. & Brodie, B. 1986. Relationship between root growth of potato, root diffusate production, and hatching of Globodera rostochiensis. *Journal of Nematology*, **18,** 379.

Ressler, D., Horton, R., Baker, J. & Kaspar, T. 1997. Testing a nitrogen fertilizer applicator designed to reduce leaching losses. *Applied Engineering in Agriculture*, **13,** 345-350.

Rice, P.J., Anderson, T.A. & Coats, J.R. 2002. Degradation and persistence of metolachlor in soil: Effects of concentration, soil moisture, soil depth, and sterilization. *Environmental toxicology and chemistry*, **21,** 2640-2648.

Robinson, D. 1999. A comparison of soil-water distribution under ridge and bed cultivated potatoes. *Agricultural Water Management*, **42,** 189-204.

Roose, T. & Fowler, A.C. 2004a. A model for water uptake by plant roots. *Journal of Theoretical Biology*, **228,** 155-171.

Roose, T. & Fowler, A.C. 2004b. A mathematical model for water and nutrient uptake by plant root systems. *Journal of Theoretical Biology*, **228,** 173-184.

Rowell, D.L., Martin, M.W. & Nye, P.H. 1967. The measurement and mechanism of ion diffusion in soils III. The effect of moisture content and soil-solution concentration on the self-diffusion of ions in soils. *Journal of Soil Science*, **18,** 204-221.

Shackelford, C.D. & Daniel, D.E. 1991. Diffusion in saturated soil. I: Background. *Journal of Geotechnical Engineering*, **117,** 467-484.

Shock, C., Feibert, E. & Saunders, L. 1998. Potato yield and quality response to deficit irrigation. *HortScience*, **33,** 655-659.

Smelt, J., Schut, C., Dekker, A. & Leistra, M. 1981. Movement and conversion of aldicarb and its oxidation products in potato fields. *Netherlands Journal of Plant Pathology*, **87,** 177-191.

Smethurst, J., Clarke, D. & Powrie, W. 2006. Seasonal changes in pore water pressure in a grass covered cut slope in London Clay. *Geotechnique*, **56,** 523-537.

Steele, D., Greenland, R. & Hatterman-Valenti, H. 2006. Furrow vs hill planting of sprinkler-irrigated russet burbank potatoes on coarse-textured soils. *American Journal of Potato Research*, **83,** 249-257.

Steudle, E., Oren, R. & Schulze, E.-D. 1987. Water transport in maize roots measurement of hydraulic conductivity, solute permeability, and of reflection coefficients of excised roots using the root pressure probe. *Plant Physiology*, **84,** 1220-1232.

Tisdall, J.M. & Hodgson, A.S. 1990. Ridge TillageRidge tillage in Australia: a review. *Soil and Tillage Research*, **18,** 127-144.

van Genuchten, M.T. 1980. A Closed-form Equation for Predicting the Hydraulic Conductivity of Unsaturated Soils1. *Soil Sci. Soc. Am. J.*, **44,** 892-898.

Wayman, J. 1969. Experiments to investigate some of the problems in mechanisation associated with the cultivation of potatoes in beds. *European Potato Journal*, **12,** 200-214.

Figure captions

Figure 1 Simulated soil domains for a ridge and furrow and flat soil geometry, where Ω and Φ are the total cross-sectional areas of the two domains, $\partial\Omega_{\mathrm{S}}$ and $\partial\Phi_{\mathrm{S}}$ are the soil surface boundaries, $\partial\Omega_{\mathrm{B}}$ and $\partial\Phi_{\mathrm{B}}$ are the base boundaries, $\partial\Omega_{\mathrm{W}}$, $\partial\Phi_{\mathrm{W}}, \partial\Omega_{\mathrm{E}}$ and $\partial\Phi_{\mathrm{E}}$ are the lateral boundaries, Ω_{A} and Φ_{A} are the areas without root activity and Ω_{U} and Φ_{U} are the areas of soil containing root activity.

Figure 2 Newbury site experimental rainfall data over a 6-month period between 1 June 2006 and 31 December 2006. The green and orange crosses indicate the time of early and late solute applications respectively.

Figure 3 Early application solute profiles in the ridged and flat domains for the moderately mobile solutes $(\gamma_1, \gamma_2, \gamma_3)$ after 16 and 24 weeks after solute application. A white contour line for the safety threshold of 10 $\mu\mathrm{g}\,\mathrm{l}^{-1}$is also plotted. The ridge and furrow and flat geometries are the same as those shown in Figure 1.

Figure 4 Early application solute profiles in the ridged and flat domains for the highly mobile solutes $(\beta_1, \beta_2, \beta_3)$ after 16 and 24 weeks after solute application. A white contour line for the safety threshold of 10 $\mu\mathrm{g}\,\mathrm{l}^{-1}$is also plotted. The ridge and furrow and flat geometries are the same as those shown in Figure 1.

Figure 5 Early application solute profiles in the ridged and flat domains for the extremely mobile solutes $(\alpha_1, \alpha_2, \alpha_3)$ after 16 and 24 weeks post solute application. A white contour line for the safety threshold of 10 μg $\mathrm{l}^{-1}$is also plotted. The ridge and furrow and flat geometries are the same as those shown in Figure 1.

Figure 6 Early and late application solute profiles in the ridged and flat domains for the slow degrading solutes α_3, β_3 and γ_3 at the end of the 24 week simulations. A white contour line for the safety threshold of 10 μg $\mathrm{l}^{-1}$is also plotted. The ridge and furrow and flat geometries are the same as those shown in Figure 1.

Figure 7 Total amount of solute leached beyond the plough layer in the ridge and furrow soil Ω and flat soil Φ for simulations that delayed the period of time between a solute application and a heavy rain event.

Table 1 Model parameter values used in numerical simulation.

Parameter	*Description*	*Value*	*Units*	*Reference*
ρ	Density of water	1×10^3	kg m^{-3}	–
g	Acceleration due to gravity	9.81	m s^{-2}	–
b	Buffer power	$0.1/1/10$	–	–
D_f	Diffusion coefficient in free liquid	2×10^{-9}	m^2 s^{-1}	(Shackelford & Daniel, 1991)
m	Van Genuchten parameter	0.5	–	(van Genuchten, 1980)
ϕ	Porosity	0.396	–	(van Genuchten, 1980)
κ_s	Saturated water permeability	5.2×10^{-14}	m^2	(van Genuchten, 1980)
p_c	Characteristic soil suction	23200	Pa	(van Genuchten, 1980)
d	Impedance factor	2	–	(Nye & Tinker, 1977; Roose & Fowler, 2004b)
μ	Viscosity of water	1×10^{-3}	kg m^{-1} s^{-1}	–
λ_c	Root surface area density water conductivity	$0 - 2.355 \times 10^{-5}$	s^{-1}MPa^{-1}	(Lesczynski & Tanner, 1976; Rawsthorne & Brodie, 1986; Steudle *et al.*, 1987; Roose & Fowler, 2004a)
p_r	Root xylem pressure	-0.05	MPa	(Liu *et al.*, 2006)
t_λ^*	Solute half-life	$10/50/500$	Days	–
I_c	Infiltration capacity	1.6×10^{-6}	m s^{-1}	(Morin & Benyamini, 1977)
A	Variation in soil depth	$0.1\dot{6}/0$	m	(Steele *et al.*, 2006; Li *et al.*, 2007)
B	Ridge wave number	$2\pi/0$	m^{-1}	(Steele *et al.*, 2006; Li *et al.*, 2007)

C	Average soil depth	$0.1\dot{6}/0$	m	(Steele *et al.*, 2006; Li *et al.*, 2007)
η	Geometry width	0.5	m	(Steele *et al.*, 2006; Li *et al.*, 2007)

Table 2 Matrix of simulated solutes used in numerical simulation.

	Extremely mobile $b = 0.1$	*Highly mobile* $b = 1$	*Moderately mobile* $b = 10$
High degradation $t_{\lambda}^{*} = 10\ days$	Solute α_1	Solute β_1	Solute γ_1
Medium degradation $t_{\lambda}^{*} = 50\ days$	Solute α_2	Solute β_2	Solute γ_2
Low degradation $t_{\lambda}^{*} = 500\ days$	Solute α_3	Solute β_3	Solute γ_3

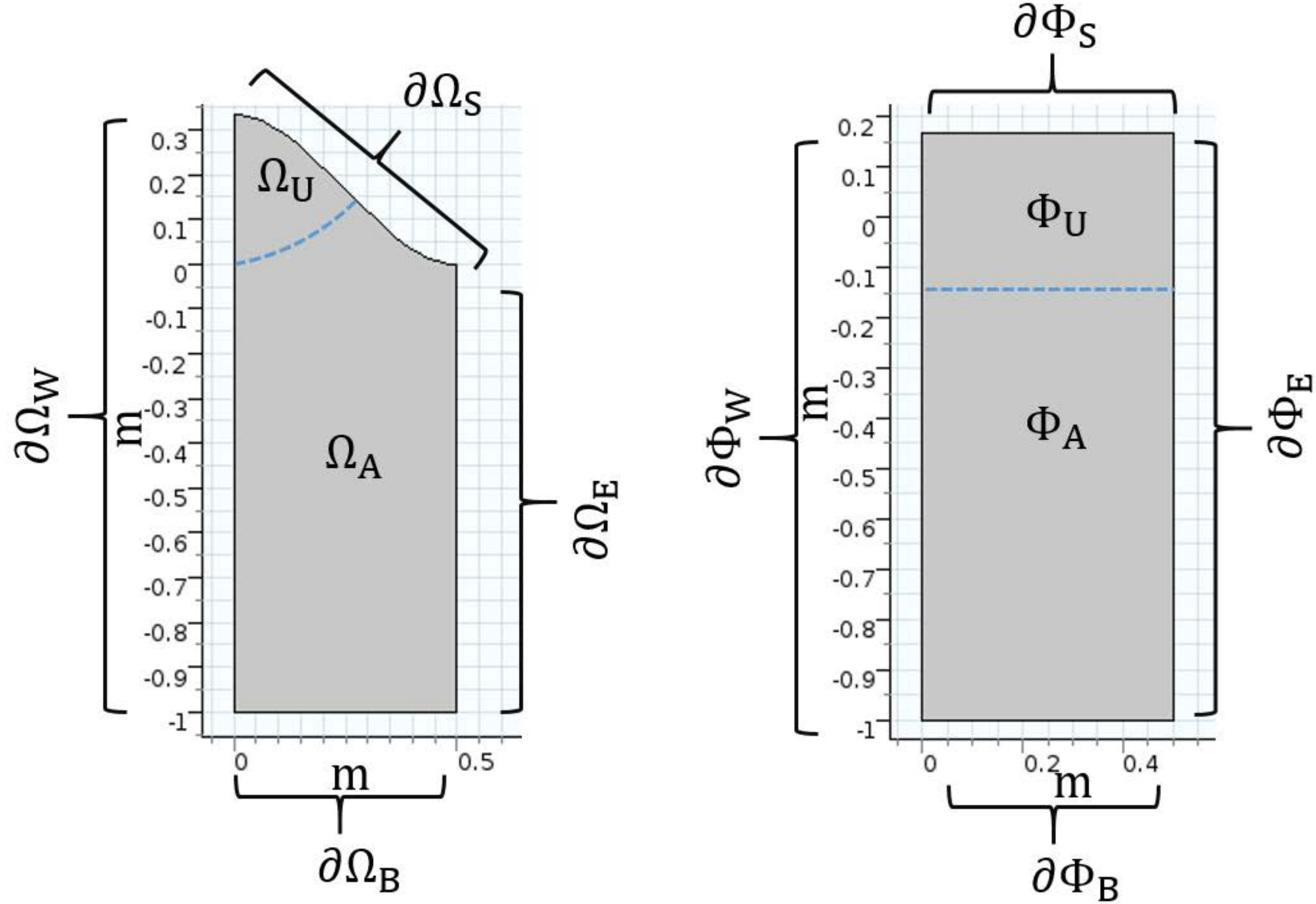

$\partial\Omega_S$
Ω_U
Ω_A
$\partial\Omega_W$
$\partial\Omega_E$
$\partial\Omega_B$
m
0.3
0.2
0.1
0
-0.1
-0.2
-0.3
-0.4
-0.5
-0.6
-0.7
-0.8
-0.9
-1
0
0.5
$\partial\Phi_S$
Φ_U
Φ_A
$\partial\Phi_W$
$\partial\Phi_E$
$\partial\Phi_B$
0.2
0.1
0
-0.1
-0.2
-0.3
-0.4
-0.5
-0.6
-0.7
-0.8
-0.9
-1
0
0.2
0.4

(a) (b)

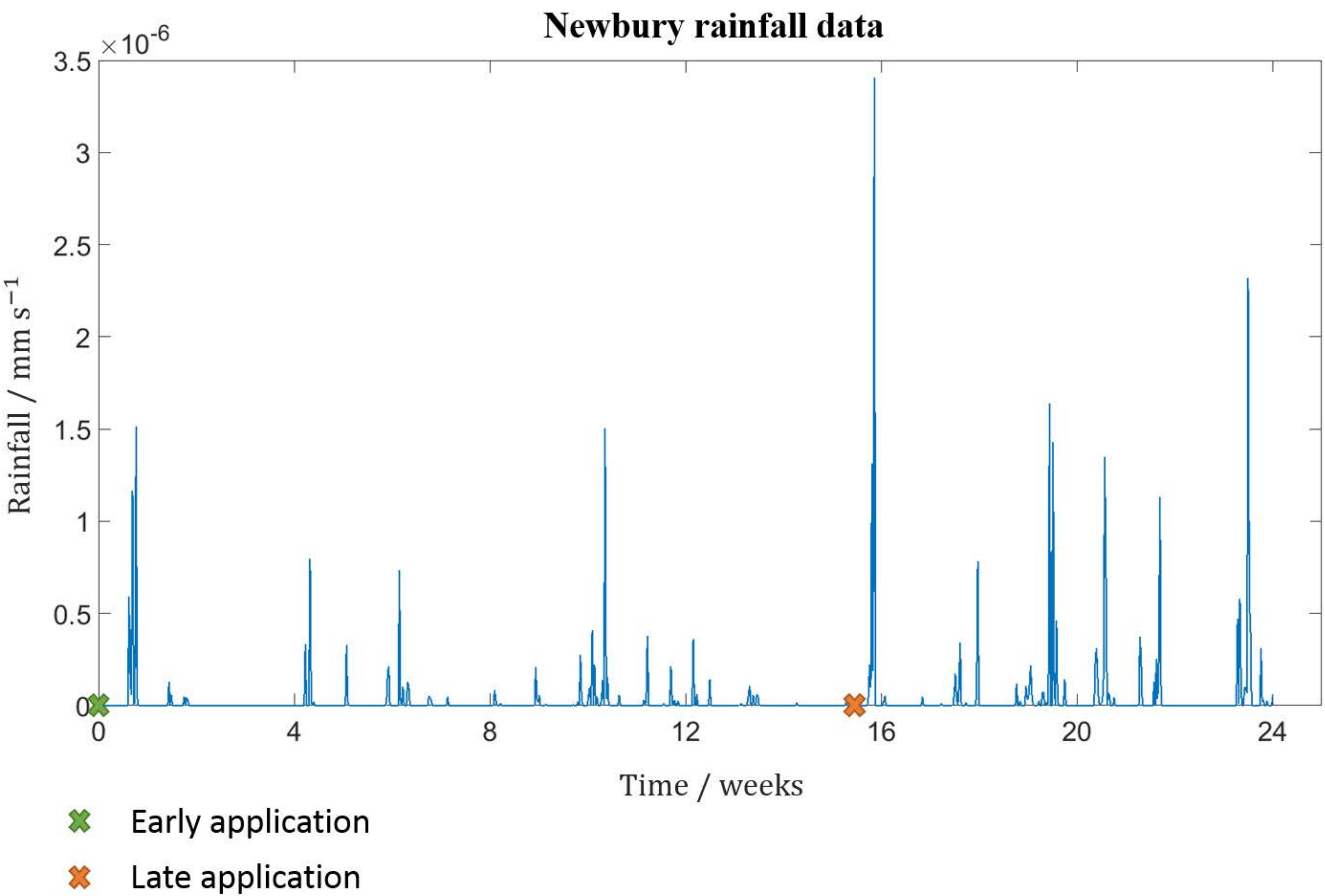

Newbury rainfall data
×10^-6
3.5
3
2.5
2
1.5
1
0.5
0
Rainfall / mm s^-1
0
4
8
12
16
20
24
Time / weeks
Early application
Late application

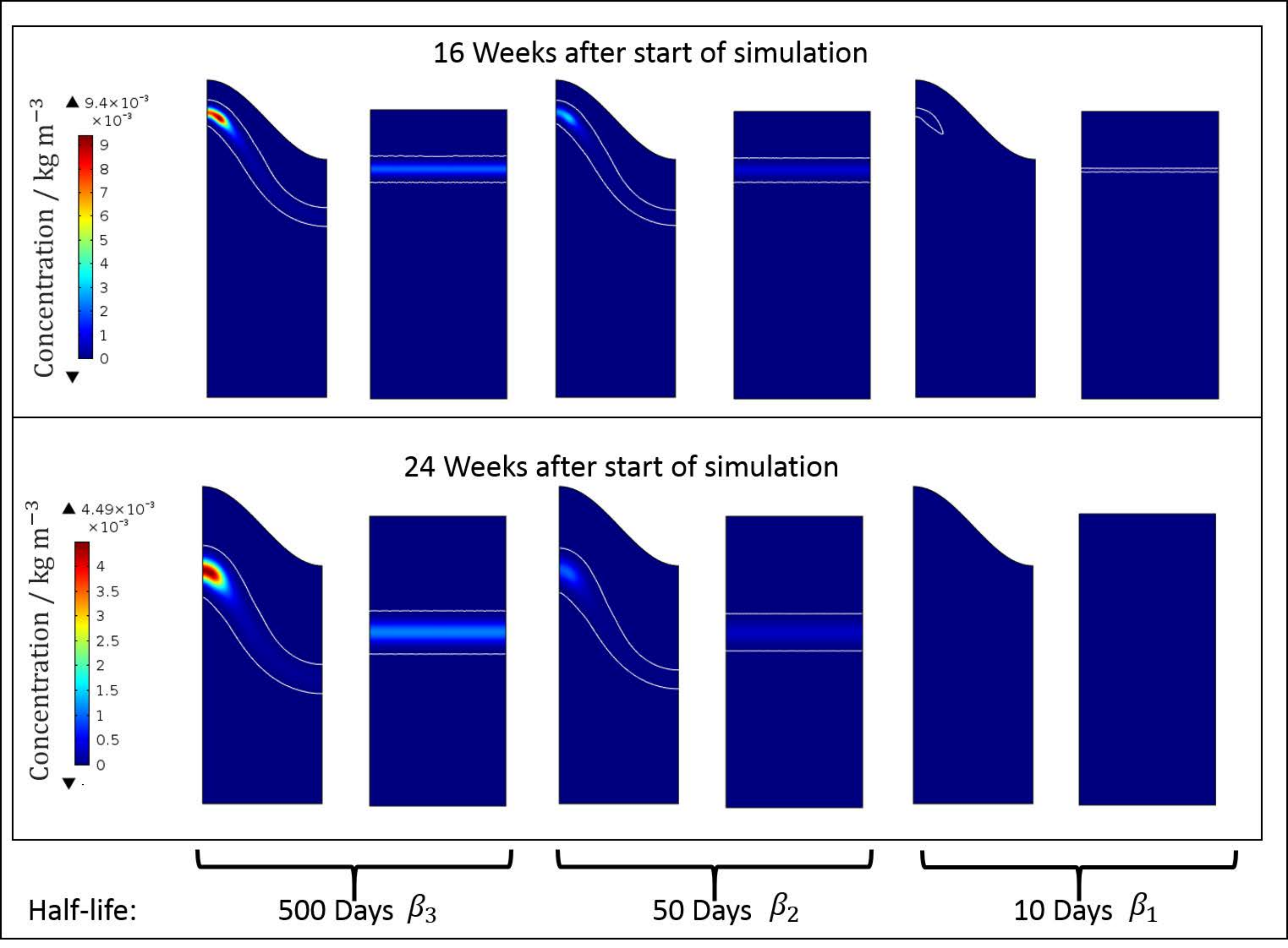

16 Weeks after start of simulation
Concentration / kg m^{-3}
9.4×10^{-3}
×10^{-3}
9
8
7
6
5
4
3
2
1
0
24 Weeks after start of simulation
Concentration / kg m^{-3}
4.49×10^{-3}
×10^{-3}
4
3.5
3
2.5
2
1.5
1
0.5
0
Half-life:
500 Days β_3
50 Days β_2
10 Days β_1

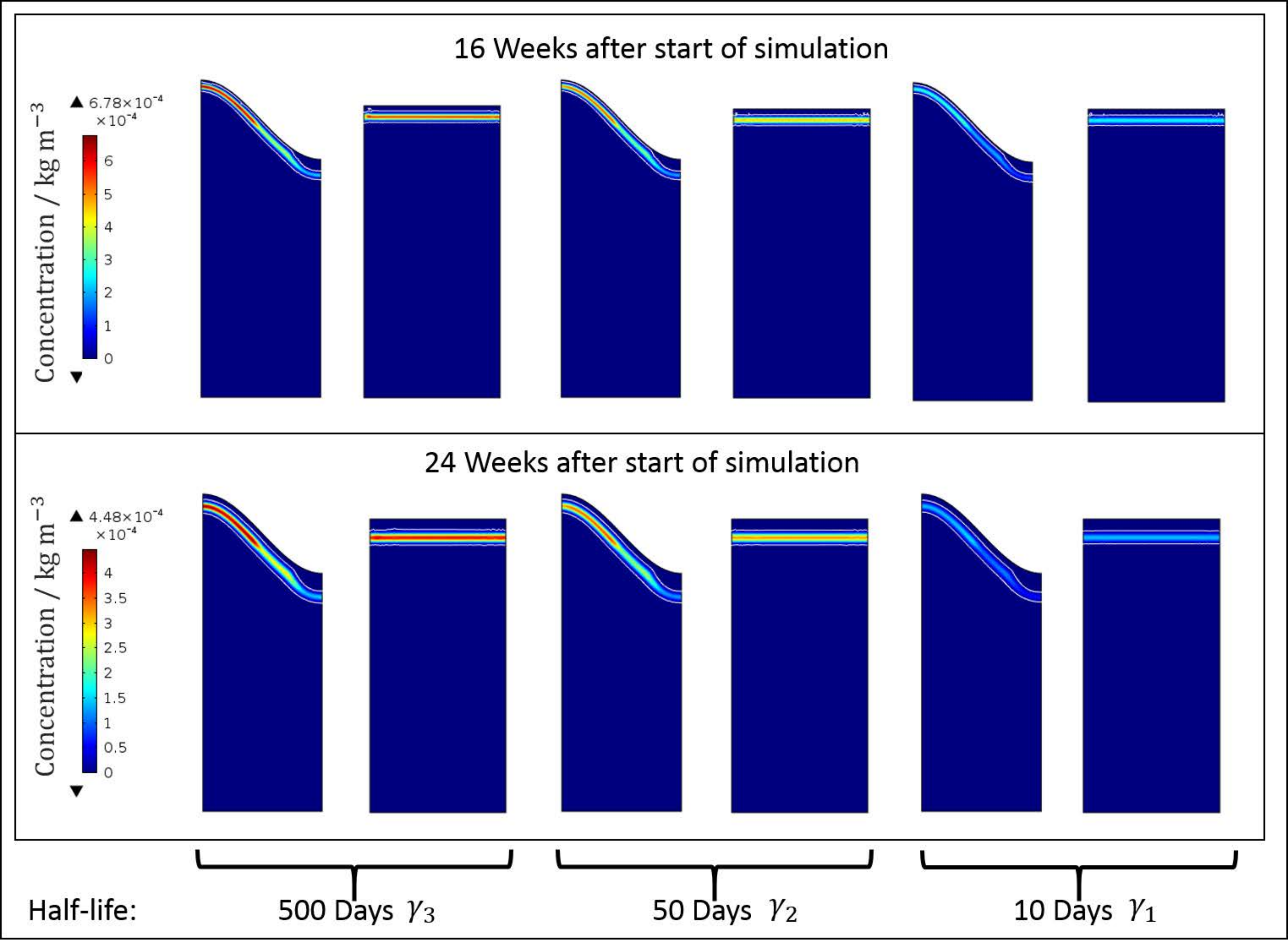

16 Weeks after start of simulation
Concentration / kg m^{-3}
6.78×10^{-4}
×10^{-4}
6
5
4
3
2
1
0
24 Weeks after start of simulation
Concentration / kg m^{-3}
4.48×10^{-4}
×10^{-4}
4
3.5
3
2.5
2
1.5
1
0.5
0
Half-life:
500 Days γ_3
50 Days γ_2
10 Days γ_1

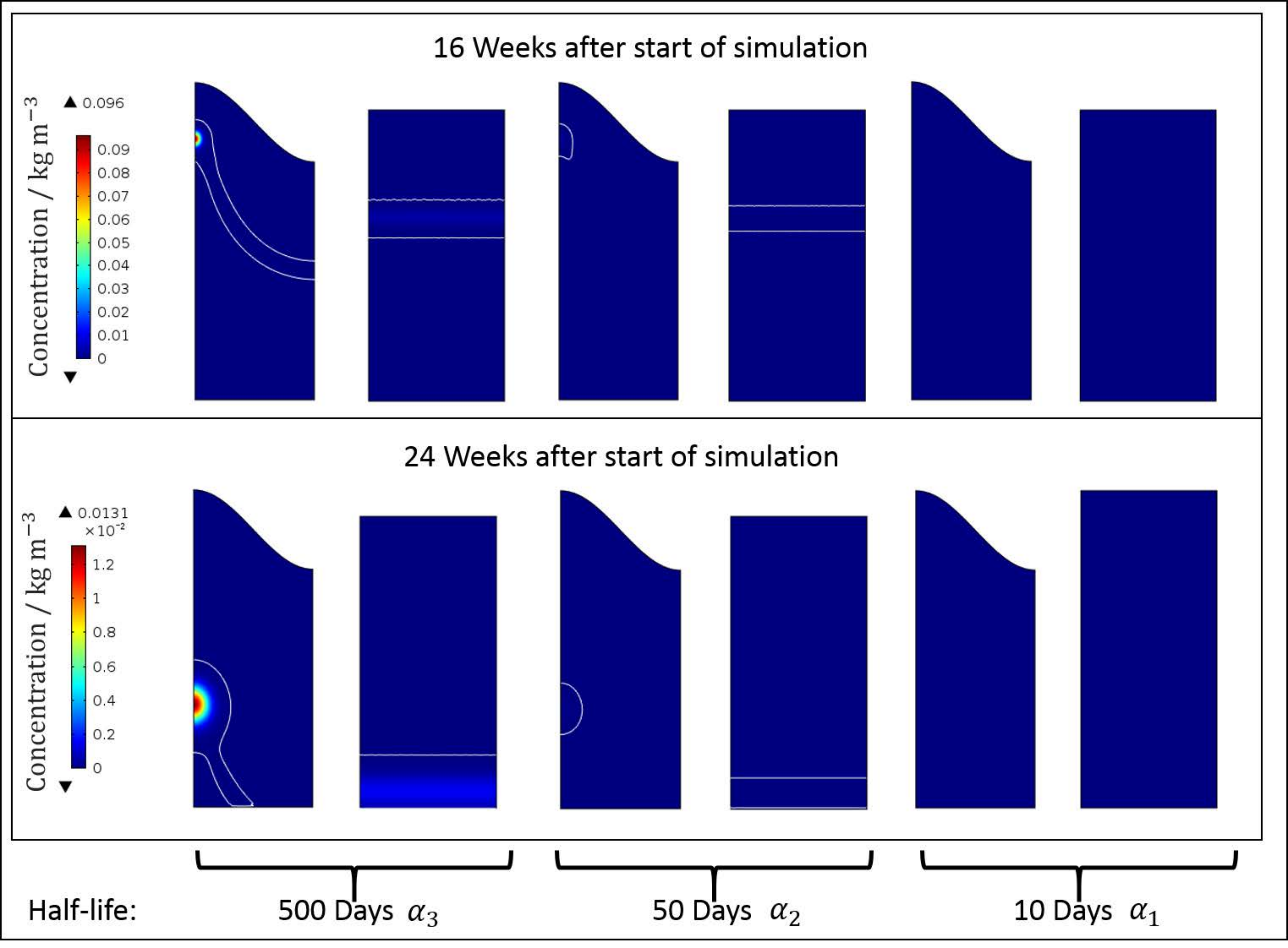
16 Weeks after start of simulation
Concentration / kg m^-3
0.096
0.09
0.08
0.07
0.06
0.05
0.04
0.03
0.02
0.01
0
24 Weeks after start of simulation
Concentration / kg m^-3
0.0131
×10^-2
1.2
1
0.8
0.6
0.4
0.2
0
Half-life:
500 Days α3
50 Days α2
10 Days α1

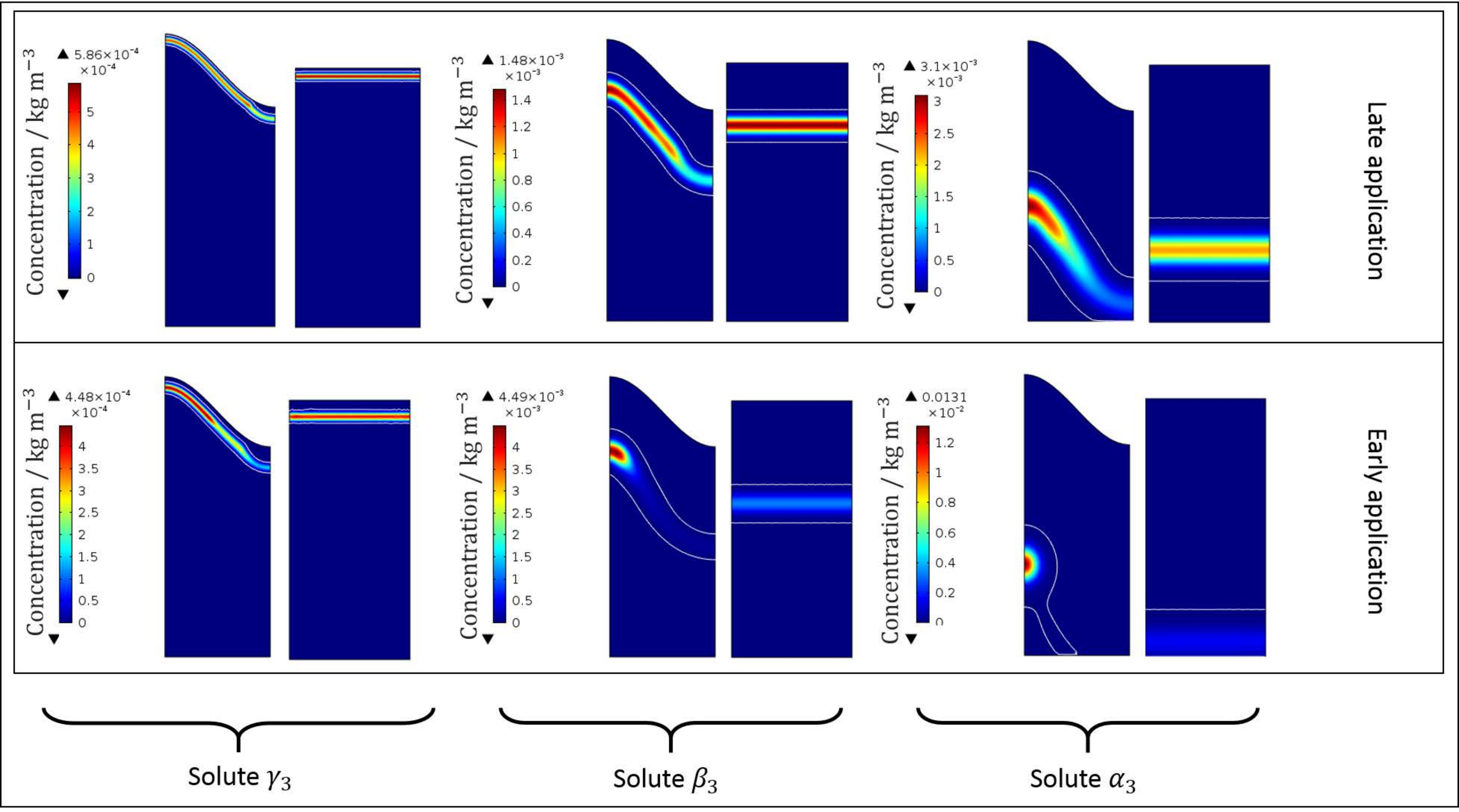
Late application
Early application
Concentration / kg m^-3
▲ 5.86×10^-4
×10^-4
5
4
3
2
1
0
▲ 1.48×10^-3
×10^-3
1.4
1.2
1
0.8
0.6
0.4
0.2
0
▲ 3.1×10^-3
×10^-3
3
2.5
2
1.5
1
0.5
0
▲ 4.48×10^-4
×10^-4
4
3.5
3
2.5
2
1.5
1
0.5
0
▲ 4.49×10^-3
×10^-3
4
3.5
3
2.5
2
1.5
1
0.5
0
▲ 0.0131
×10^-2
1.2
1
0.8
0.6
0.4
0.2
0
Solute γ_3
Solute β_3
Solute α_3

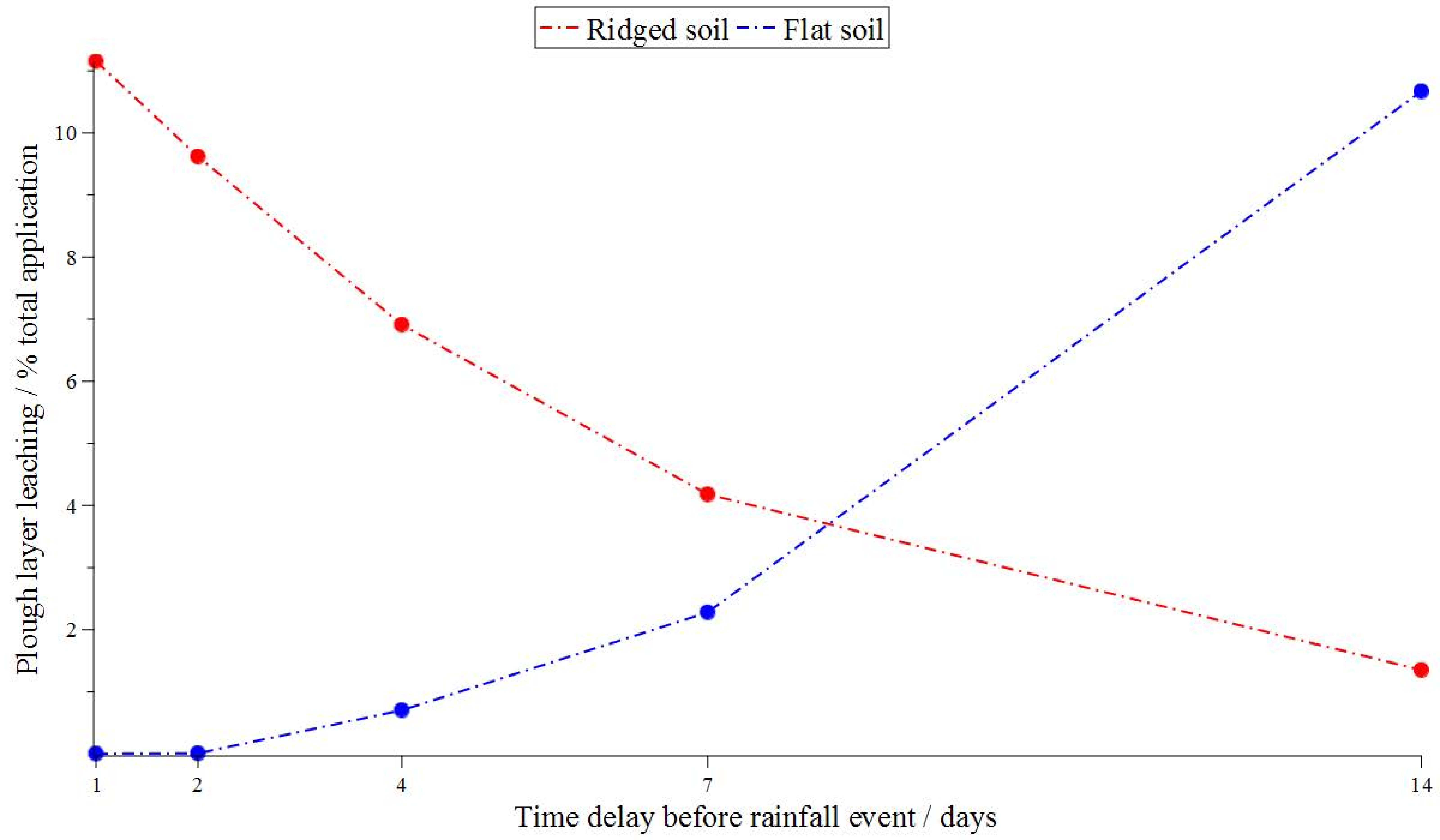

Ridged soil
Flat soil
Plough layer leaching / % total application
10
8
6
4
2
1
2
4
7
14
Time delay before rainfall event / days